

Research Article

Single and Binary Adsorption Systems of Rhodamine B and Methylene Blue onto Alkali-Activated Vietnamese Diatomite

Pham Dinh Du ¹ and Huynh Thanh Danh ²

¹Thu Dau Mot University, Binh Duong 75000, Vietnam

²Giong Rieng High School, Kien Giang 91000, Vietnam

Correspondence should be addressed to Pham Dinh Du; dupd@tdmu.edu.vn

Received 17 May 2021; Accepted 1 June 2021; Published 5 July 2021

Academic Editor: Susana Silva-Martinez

Copyright © 2021 Pham Dinh Du and Huynh Thanh Danh. This is an open access article distributed under the Creative Commons Attribution License, which permits unrestricted use, distribution, and reproduction in any medium, provided the original work is properly cited.

Diatomite was slightly modified with a sodium hydroxide solution. The resulting material was characterized by using energy-dispersive X-ray spectroscopy (EDX), X-ray diffraction (XRD), Fourier-transform infrared spectroscopy (FT-IR), scanning electron microscopy (SEM), and nitrogen adsorption-desorption isotherms. The so-treated diatomite has a high specific surface area ($77.8 \text{ m}^2/\text{g}$) and a high concentration of isolated silanol groups on the surface, and therefore, its adsorption capacity increases drastically in both the single and binary adsorption systems for rhodamine B and methylene blue. The binary system is more effective than the single system, with methylene blue being adsorbed more than rhodamine B. The adsorption process is spontaneous and fits well with the Langmuir isothermal model, and it depends on pH significantly.

1. Introduction

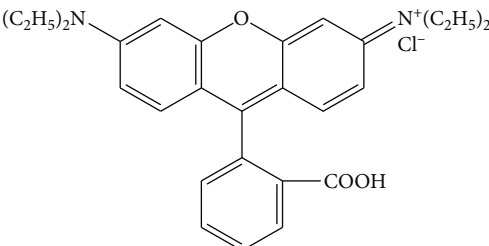
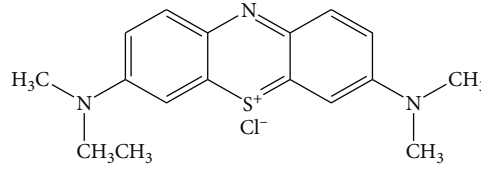
Dyes are widely used in numerous applications, such as textile, paper, plastic, and dye industries [1]. The amount of dyes produced annually worldwide is estimated at over 7×10^5 tons, and more than 100,000 commercially available dyes with different physical and chemical properties are being used [2–4]. Various dyes and their decomposition products are toxic and carcinogenic, thus posing a danger to aquatic organisms [1, 5]. Therefore, dye removal from wastewater is essential.

A large number of dyes have a complex aromatic ring structure and are difficult to degrade biologically [4, 6]. Therefore, it is necessary to reduce their concentration in wastewaters prior to biological treatment. Chemical oxidation has been extensively studied for dye removal from wastewaters [1, 7–9]. However, oxidation often produces intermediate products that can cause secondary pollution. Meanwhile, the adsorption technique has proven to be a simple, efficient, and attractive way to remove nonbiodegradable pollutants (including dyes) from wastewaters [5, 10, 11].

To remove dyes from complex aqueous solutions, a variety of adsorbents have been used, such as banyan aerial roots [12], peat [2], bentonite [13], mesoporous silica nanoparticles [14], clay [15, 16], activated banana peel carbon [17], silica extracted from rice husk [18], and zeolite [19], and some of them exhibit high performance. However, the search for new, effective, cheap, and environmentally friendly adsorbents is on the way.

Diatomite is a low-density, small-particle sedimentary rock consisting mainly of amorphous silica ($\text{SiO}_2 \cdot n\text{H}_2\text{O}$) derived from diatoms. Diatomite encompasses a variety of structures and has high porosity (up to 80%), a large specific surface area, and multiple hydroxyl groups on the surface [3, 6, 10, 11, 20]. These properties enable diatomite to be a potential adsorbent for the pollutants present in industrial wastewaters, including dyes. Besides, diatomite is abundant in nature, cheap, and environmentally friendly [11]. Several studies have dealt with the applicability of natural diatomite in the adsorption field [6, 10, 11, 21–23]. Other studies have focused on diatomite surface modification with metals or organic functional groups to improve adsorption efficiency

TABLE 1: Main characteristics of the dyes used in this study.

| Dye | RB | MB |
|--------------------------|---|--|
| Type | Basic violet 10, C.I.45170, cationic | Basic blue 9, C.I.52015, cationic |
| Phase | Solid | Solid |
| Molecular formula | $C_{28}H_{31}O_3N_2Cl$ | $C_{16}H_{18}N_3S^+Cl^-$ |
| Molecular weight (g/mol) | 479.03 | 319.85 |
| Chemical structure |  |  |

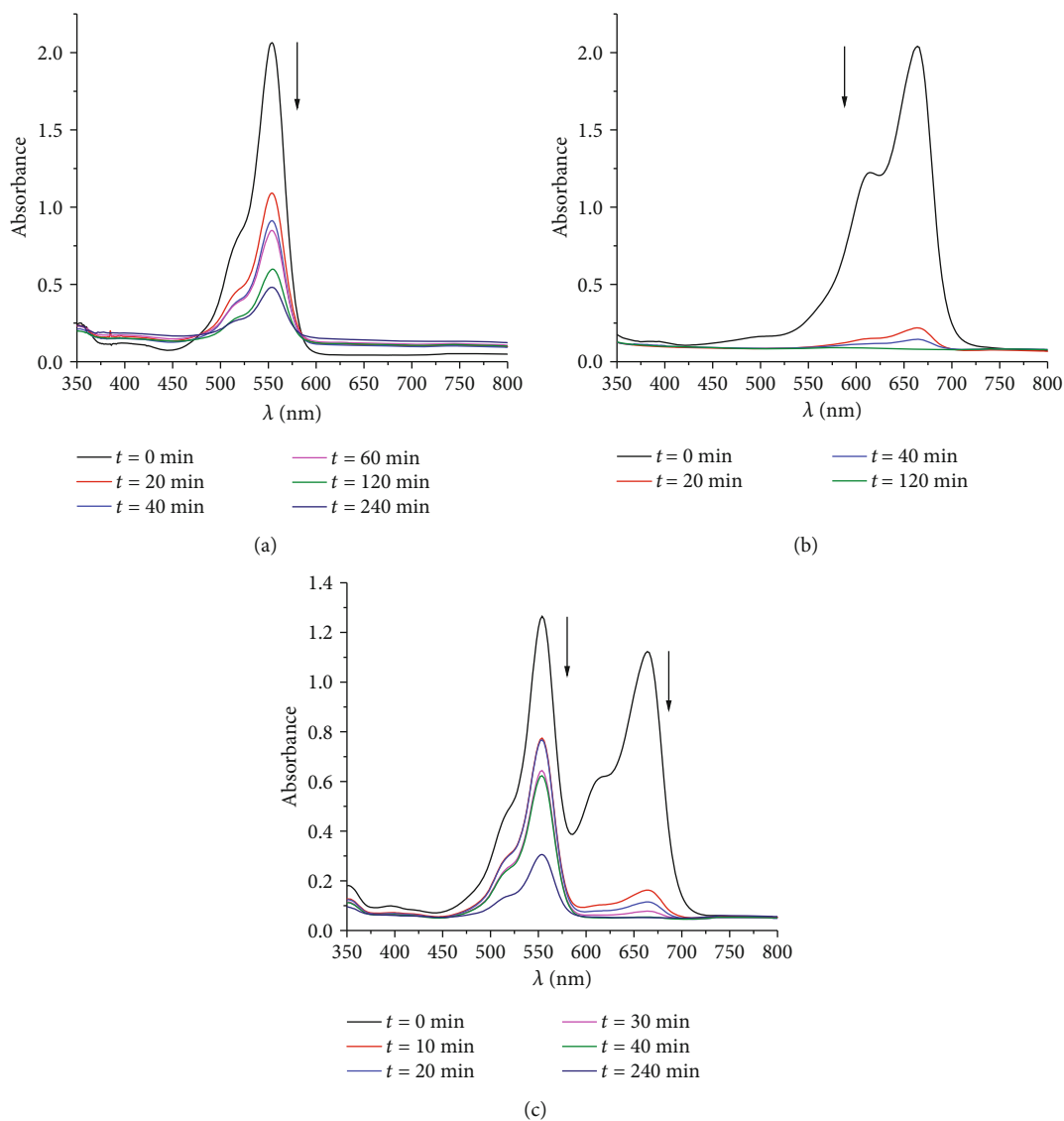


FIGURE 1: UV-Vis absorption spectra for aqueous solutions of (a) RB, (b) MB, and (c) both of the dyes along with alkali-activated diatomite at various adsorption times.

or expand its applications [1, 7–9, 24–32]. In some studies, natural diatomite is treated thermally [3, 10, 20, 33, 34], with acids [3, 20, 35–37], or with alkalines [4, 37, 38] to enhance its application performance. Other studies use diatomite as a raw material to manufacture other products [14, 35, 39–42]. The diatomite purified by calcining is also investigated by Yuan et al. [43]. They discovered that when the temperature increases, the condensation of surface silanol groups occurs. Hydrogen-linked hydroxyl groups condense more easily than isolated hydroxyl groups. Bronsted acid centers also condense at high temperatures. This condensation reduces the adsorption capacity of the diatomite treated by calcining toward base dyes. When treated with acids (normally at high concentration: 5 M H_2SO_4 [3], 5 M HCl [35], 1–5 M HCl [36], 10% HCl [20], and 1 M H_2SO_4 [37]), it is difficult to perform the modification and is easily contaminated by secondary pollution. Therefore, numerous studies have focused only on diatomite purification because it is cheap, easy to operate, and environmentally friendly [4]. When purified with alkali, diatomite retains its hydroxyl groups on the surface, and they are excellent adsorption centers for many metals as well as dyes.

Since most industrial wastewaters contain different pollutants, it is important to investigate the effect of multicomponent systems on the adsorption capacity. Various studies have studied the simultaneous removal of different pollutants from aqueous solutions [2, 5, 44] to assess the competitiveness of adsorbates. In this study, natural diatomite is activated by treating with low-concentrated sodium hydroxide to enhance the adsorption capacity for rhodamine B (RB) and methylene blue (MB) in single and binary systems. The equilibrium isotherms and thermodynamic parameters of the adsorption processes are studied. In addition, the effect of the solution pH on the adsorption efficiency of RB or MB in the single system is also investigated.

2. Materials and Methods

2.1. Materials. Natural diatomite was obtained from Phu Yen province, Vietnam. Natural diatomite was washed several times with water, dried at 100°C , sieved, and stored in closed containers for further tests. The product is called purified diatomite.

Sodium hydroxide (NaOH), hydrochloric acid (HCl), and potassium chloride (KCl) were purchased from Guangdong (China). Methylene blue (Guangdong, China) and rhodamine B (HiMedia, India) dyes were used as adsorbates. A summary of the main characteristics of these dyes is given in Table 1 [3, 5, 22, 27, 37].

2.2. Activation of Diatomite. Purified diatomite was activated with NaOH to enhance the adsorption capacity. The purified diatomite sample was immersed in a 5% NaOH solution at a ratio of 1 : 10 (w/w) and stirred at 100°C for 2 h to remove impurities and organics. Then, the solid was filtered, washed several times with distilled water, dried at 100°C , and sieved. The obtained alkali-activated diatomite was stored in closed containers for further tests.

TABLE 2: Elemental composition of the diatomite samples ($w\%$, EDX).

| Element | Purified diatomite | Alkali-activated diatomite |
|---------|--------------------|----------------------------|
| O | 52.72 ± 1.48 | 49.06 ± 1.27 |
| Mg | 0.53 ± 0.06 | 0.53 ± 0.04 |
| Al | 10.36 ± 0.87 | 11.59 ± 0.03 |
| Si | 30.56 ± 0.59 | 27.50 ± 1.42 |
| K | 0.20 ± 0.09 | 1.09 ± 0.83 |
| Ca | 0.21 ± 0.05 | 0.17 ± 0.03 |
| Ti | 0.91 ± 0.17 | 1.23 ± 0.10 |
| Fe | 4.50 ± 0.10 | 6.02 ± 0.27 |
| Na | — | 1.77 ± 0.24 |
| Cl | — | 1.03 ± 0.19 |
| Total | 100 | 100 |

2.3. Characterization. The chemical analysis of diatomite was performed by using energy-dispersive X-ray spectroscopy (EDX, JEOL JED-2300, Japan) at different sites of the material. The powder X-ray diffraction (XRD) patterns were recorded by VNU-D8 Advance, Bruker, Germany, with $\text{Cu K}\alpha$ radiation ($\lambda = 1.5406 \text{ \AA}$). Fourier-transform infrared spectra (FT-IR) were measured on a Jasco FT/IR-4600 spectrometer (Japan) with a range of $4000\text{--}400 \text{ cm}^{-1}$. The morphology of diatomite was observed with scanning electron microscopy (SEM) using SEM JMS-5300LV (Japan). Nitrogen adsorption/desorption isotherm measurements were conducted using a TriStar 3000 analyzer. Samples were pretreated by heating at 250°C for 5 h with N_2 before the measurements.

2.4. Point of Zero Charge. The point of zero charge (pH_{PZC}) of the adsorbent was determined to follow the methods of Mahmood et al. [45], Jing et al. [46], and Du and Hoai [47]. To a series of 100 mL Erlenmeyer flasks, 50 mL of a 0.01 M KCl solution was added. The initial pH (pH_i) of the solutions was adjusted, ranging from 2 to 12, by adding a 0.1 M HCl or 0.1 M NaOH solution. Then, 0.1 g of the adsorbent was added to each flask and mixtures were shaken for 48 h. The final pH (pH_f) of the solutions was measured. The difference between the final and initial pHs ($\Delta\text{pH} = \text{pH}_f - \text{pH}_i$) was plotted against the pH_i . The point of intersection of the curve with the abscissa, at which $\Delta\text{pH} = 0$, provides pH_{PZC} .

2.5. Adsorption

2.5.1. Adsorption Experiments. Adsorption experiments were carried out with a typical batch approach in a 250 mL round flask with a reflux condenser. In each experiment, 0.02 g of the adsorbent was stirred with 100 mL of a solution containing RB (or MB or a mixture of RB and MB) at a specific concentration, and the temperature of the reactor was fixed at 30 or 45°C . After a certain interval, 5 mL of the solution was withdrawn and centrifuged to remove the adsorbent, and the concentration of the remaining solution was determined. The concentration of dyes was determined with the UV-Vis

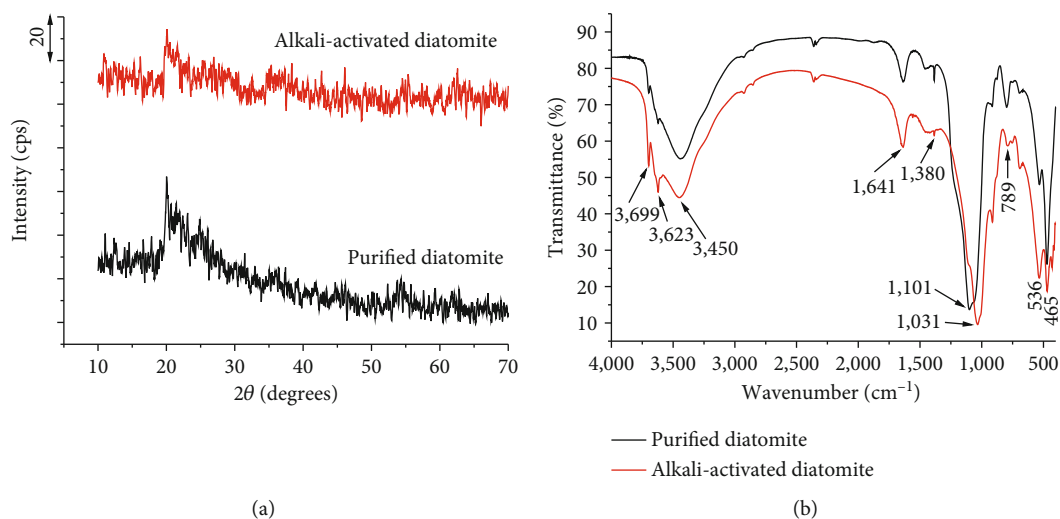


FIGURE 2: XRD pattern (a) and FT-IR spectra (b) of the diatomite samples.

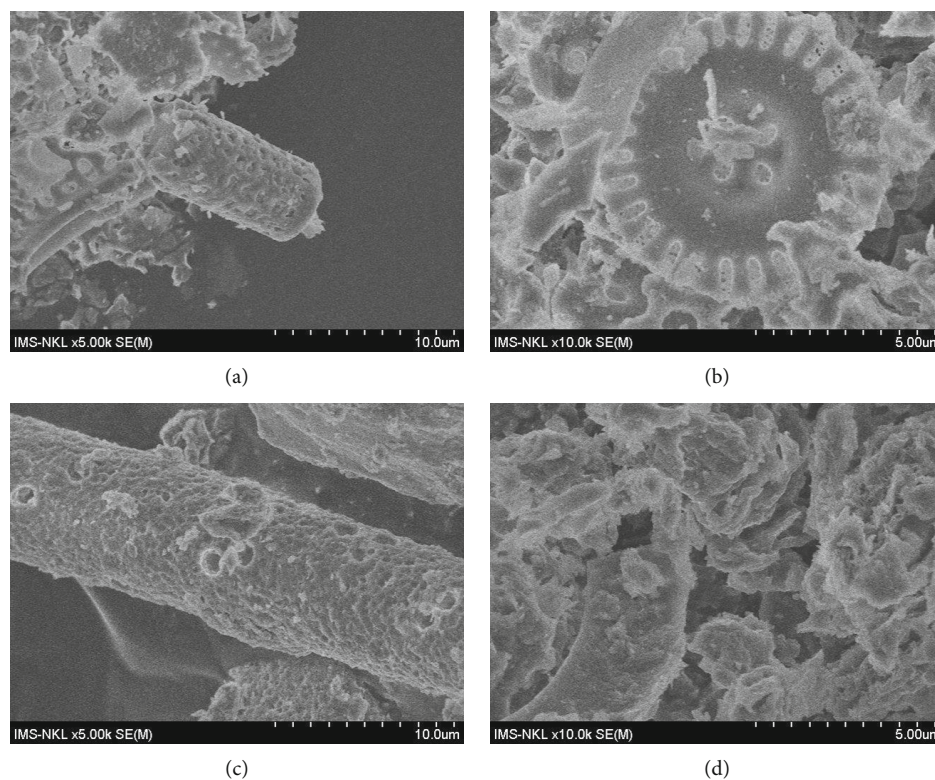


FIGURE 3: SEM images. (a, b) Purified diatomite. (c, d) Alkali-activated diatomite.

method on UVD-3000 (Labomed, USA) at $\lambda_{\max} = 554$ nm for RB and $\lambda_{\max} = 664$ nm for MB (Figure 1). The adsorbed capacity (q_t or q_e) and removal efficiency (R) of the dye adsorbed onto the adsorbent were calculated according to the following equations:

$$q_t = \frac{(C_0 - C_t) \times V}{m} \text{ (mol} \cdot \text{g}^{-1}\text{)}, \quad (1)$$

$$q_e = \frac{(C_0 - C_e) \times V}{m} \text{ (mol} \cdot \text{g}^{-1}\text{)}, \quad (2)$$

$$R = \frac{(C_0 - C_e)}{C_0} \times 100 \text{ (\%)}, \quad (3)$$

where C_0 and C_t are the concentrations of the dyes in the solution ($\text{mol} \cdot \text{L}^{-1}$) at time $t = 0$ and $t = t$, respectively; C_e is the concentration of the dyes in the solution ($\text{mol} \cdot \text{L}^{-1}$) at

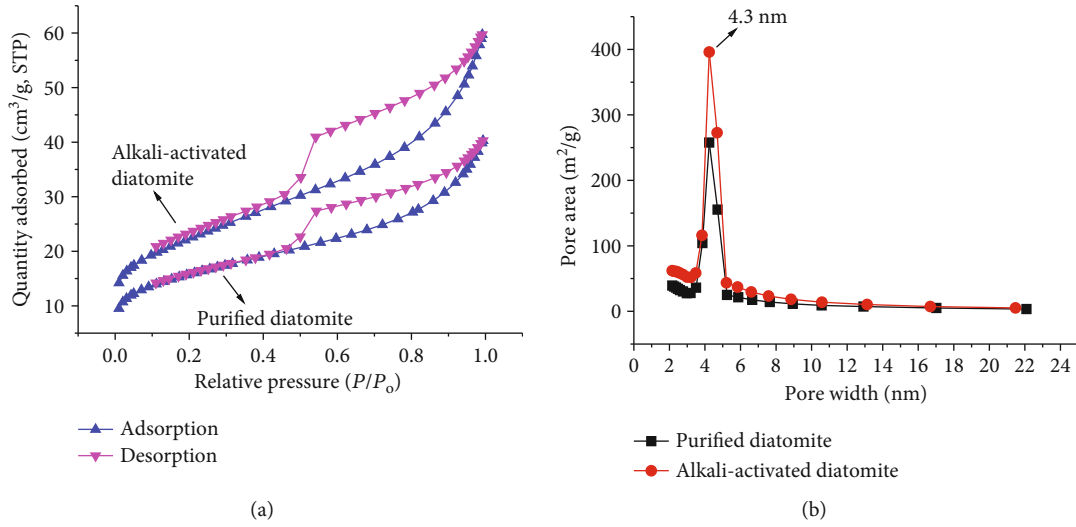


FIGURE 4: Nitrogen adsorption-desorption isotherms (a) and pore size distributions (b) of the diatomite samples.

TABLE 3: Textural properties of the diatomite samples.

| Sample | S_{BET} ($\text{m}^2 \cdot \text{g}^{-1}$) | S_{mic} ($\text{m}^2 \cdot \text{g}^{-1}$) | S_{ext} ($\text{m}^2 \cdot \text{g}^{-1}$) | V_{mic} ($\text{cm}^3 \cdot \text{g}^{-1}$) | V_{tot} ($\text{cm}^3 \cdot \text{g}^{-1}$) |
|----------------------------|---|---|---|--|--|
| Purified diatomite | 55.4 | 19.2 | 36.2 | 0.0088 | 0.0623 |
| Alkali-activated diatomite | 77.8 | 19.7 | 59.1 | 0.0089 | 0.0924 |

equilibrium; V is the volume of the solution (L); and m is the weight of the dry adsorbent (g).

The influence of initial pH (3, 5, 7, 9, and 11) was also studied in a single system with a similar procedure.

2.5.2. Isothermal Models. In this work, the Langmuir and Freundlich two-parameter models were used to analyze the adsorption equilibrium data.

The Langmuir model is based on the assumption that the adsorption is a monolayer; that is, the adsorbates form a monolayer and all the sorption sites on the adsorbent surface have the same affinity for the adsorbates. The Langmuir isotherm equation [48] is as follows:

$$q_e = q_m \times \frac{K_L \times C_e}{1 + K_L \times C_e}, \quad (4)$$

where q_m is the maximum monolayer adsorption capacity of the adsorbent ($\text{mol} \cdot \text{g}^{-1}$) and K_L is the Langmuir constant ($\text{L} \cdot \text{mol}^{-1}$). The other parameters are described above. The Langmuir constant is a measure of the affinity between the adsorbate and the adsorbent and relates to the free energy of adsorption [5]. The most commonly used linear form of the Langmuir equation [2–5, 13, 18, 20, 32, 42, 49–51] is

$$\frac{C_e}{q_e} = \frac{1}{q_m} \times C_e + \frac{1}{K_L \times q_m}. \quad (5)$$

The plot of C_e/q_e versus C_e is a straight line with the slope $1/q_m$ and intercept $1/(q_m \cdot K_L)$.

The Freundlich expression is an exponential equation and therefore assumes that as the adsorbate concentration

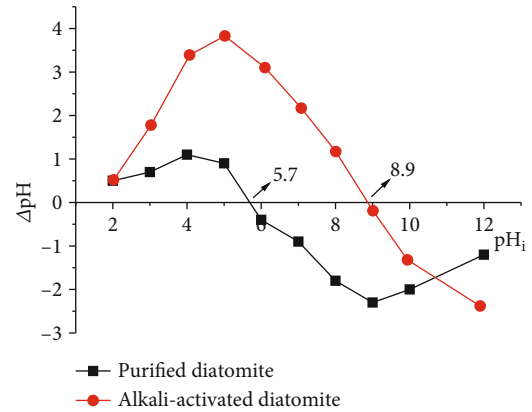


FIGURE 5: Determination of the point of zero charge of the diatomite samples.

increases, the concentration of the adsorbate on the adsorbent surface also increases. The Freundlich isotherm is expressed by the following empirical equation [48]:

$$q_e = K_F \times C_e^{1/n}, \quad (6)$$

where n is the heterogeneity factor, and K_F is the Freundlich constant ($\text{mol}^{(1-1/n)} \cdot \text{L}^{1/n} \cdot \text{g}^{-1}$). n and K_F are dependent on temperature; n indicates the extent of the adsorption, and K_F expresses the degree of nonlinearity between the solution concentration and the adsorption.

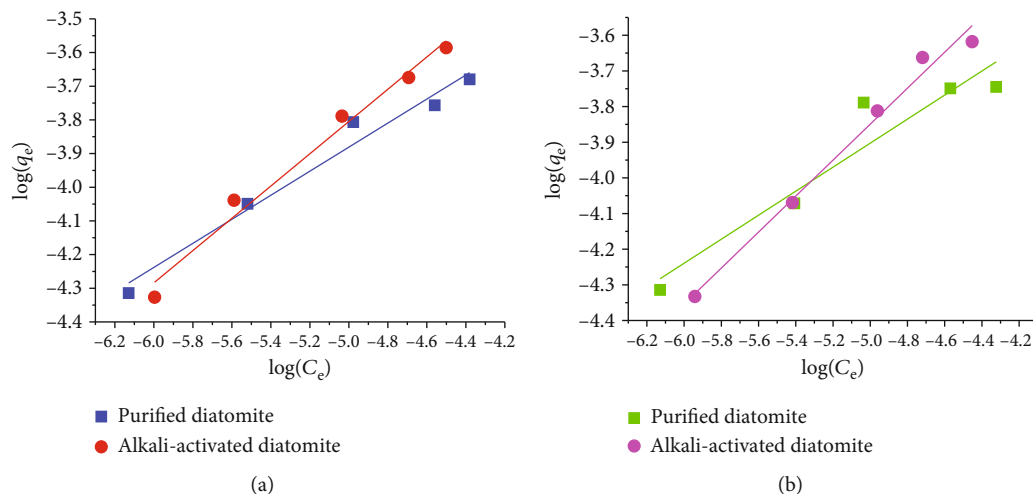


FIGURE 6: Freundlich isothermal model for RB adsorption onto diatomite: (a) 30°C and (b) 45°C.

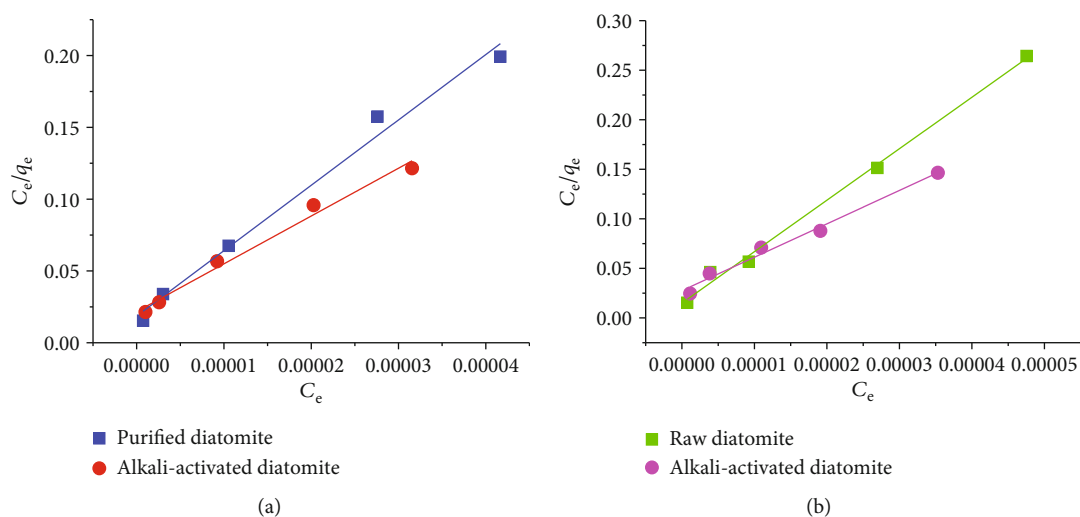


FIGURE 7: Langmuir isothermal model for RB adsorption onto diatomite: (a) 30°C and (b) 45°C.

TABLE 4: Isotherm parameters for adsorption of RB onto the diatomite.

| Sample | Temperature (°C) | n | Freundlich K_F | R^2 | q_{\max} (mol·g ⁻¹) | Langmuir K_L | R^2 |
|----------------------------|------------------|------|------------------------|--------|-----------------------------------|--------------------|--------|
| Purified diatomite | 30 | 2.80 | 8.02×10^{-3} | 0.9738 | 2.20×10^{-4} | 2.45×10^5 | 0.9880 |
| | 45 | 2.97 | 6.05×10^{-3} | 0.9104 | 1.93×10^{-4} | 3.49×10^5 | 0.9955 |
| Alkali-activated diatomite | 30 | 2.09 | 38.98×10^{-3} | 0.9833 | 3.00×10^{-4} | 1.53×10^5 | 0.9857 |
| | 45 | 1.98 | 47.23×10^{-3} | 0.9874 | 2.97×10^{-4} | 1.23×10^5 | 0.9856 |

The linear form of the Freundlich equation is

$$\log(q_e) = \log(K_F) + \frac{1}{n} \times \log(C_e). \quad (7)$$

The plot of $\log(q_e)$ versus $\log(C_e)$ is a straight line with the slope $1/n$ and intercept $\log(K_F)$.

2.5.3. Thermodynamic Parameters. To determine whether the adsorption process occurs spontaneously or not, we have to study the thermodynamic parameters. At equilibrium, the Gibbs free energy of adsorption (ΔG°) is an important quantity for determining the spontaneity of the process itself and is calculated according to the following equation:

$$\Delta G^\circ = -R \times T \times \ln K_e, \quad (8)$$

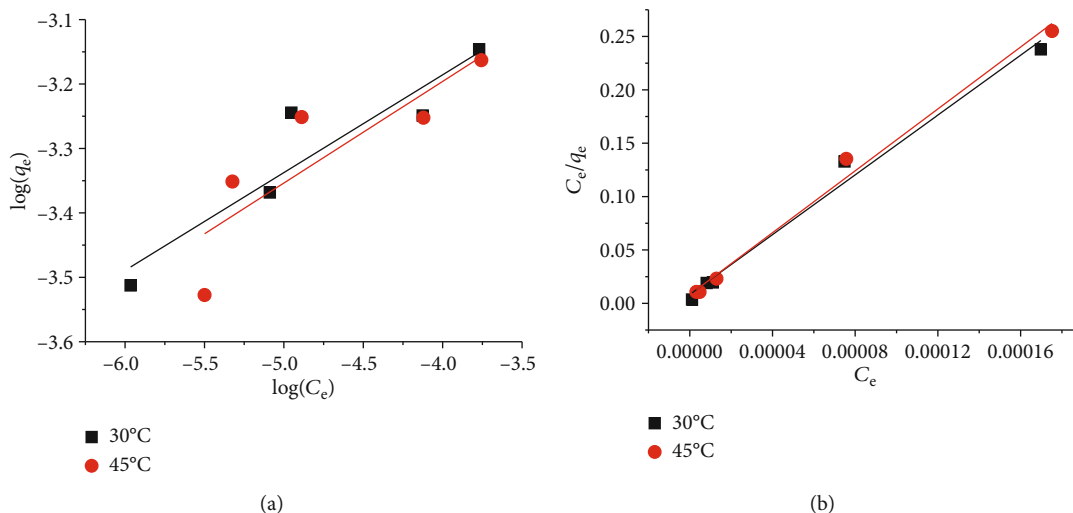


FIGURE 8: Plots of the isothermal equations in the linear form for MB adsorption onto alkali-activated diatomite at different temperatures in the single systems: (a) Freundlich and (b) Langmuir.

TABLE 5: Isotherm parameters for adsorption of MB onto alkali-activated diatomite in the single systems.

| Temperature (°C) | <i>n</i> | Freundlich | | <i>q</i> _{max} (mol·g ⁻¹) | Langmuir | |
|------------------|----------|-------------------------|-----------------------|--|------------------------|-----------------------|
| | | <i>K</i> _F | <i>R</i> ² | | <i>K</i> _L | <i>R</i> ² |
| 30 | 6.59 | 2.64 × 10 ⁻³ | 0.8676 | 7.14 × 10 ⁻⁴ | 1.69 × 10 ⁵ | 0.9874 |
| 45 | 6.34 | 2.72 × 10 ⁻³ | 0.7353 | 6.90 × 10 ⁻⁴ | 1.77 × 10 ⁵ | 0.9915 |

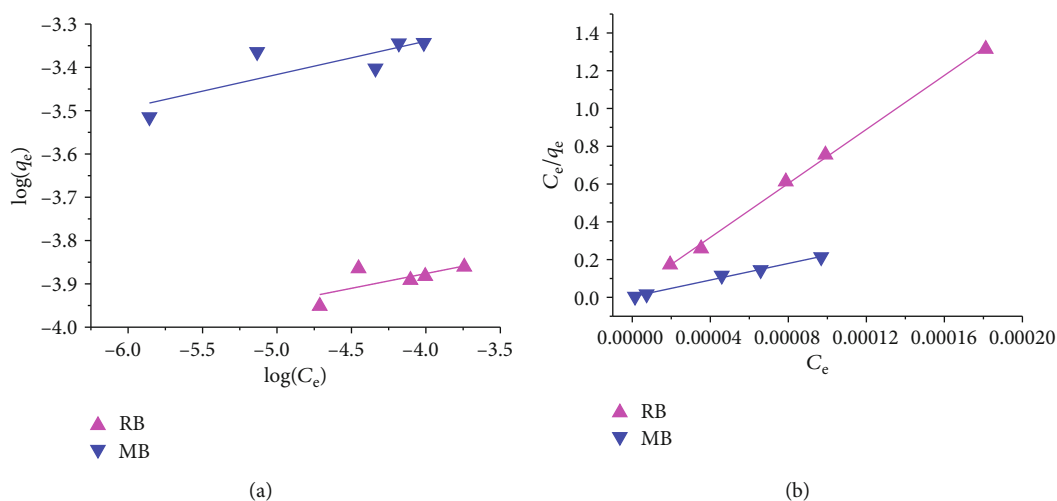


FIGURE 9: Plots of the isothermal equations in the linear form for the adsorption onto alkali-activated diatomite in the binary systems at 30°C: (a) Freundlich and (b) Langmuir.

where K_e is the thermodynamic equilibrium constant; R is the universal gas constant (8.314 J·mol⁻¹·K⁻¹); and T is the absolute temperature in Kelvin.

For the adsorption process, K_e can be determined in a number of ways, depending on the experimental conditions, such as the equilibrium constant $K_C = (C_0 - C_e)/C_e$ [3, 16, 18, 20, 38], the distribution coefficient $K_d = q_e/C_e$ [12–14, 34, 37, 42, 50–52], and the Langmuir constant K_L [4–6, 53, 54].

In this study, the adsorption constant in the Langmuir isotherm (K_L) was used to determine thermodynamic parameters (ΔG° , ΔH° , and ΔS°) for the adsorption by using the following equations [5]:

$$\Delta G^\circ = -R \times T \times \ln K_L, \tag{9}$$

$$\Delta H^\circ = -R \times \left(\frac{T_2 \times T_1}{T_2 - T_1} \right) \times \ln \frac{K_{L1}}{K_{L2}}, \tag{10}$$

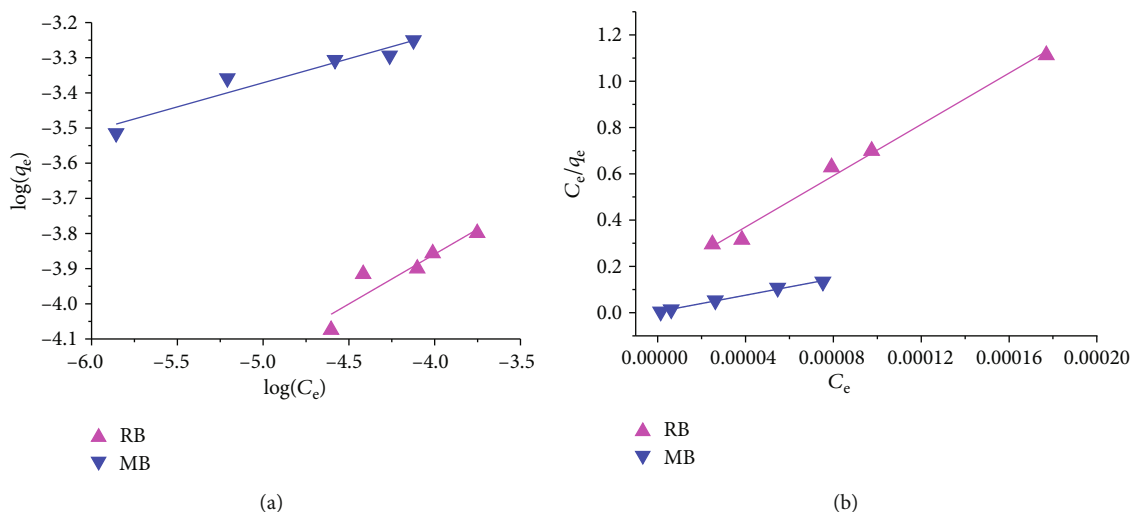


FIGURE 10: Plots of the isothermal equations in the linear form for the adsorption onto alkali-activated diatomite in the binary systems at 45°C: (a) Freundlich and (b) Langmuir.

$$\Delta S^\circ = \frac{\Delta H^\circ - \Delta G^\circ}{T}, \quad (11)$$

where K_{L1} and K_{L2} are adsorption Langmuir constants at T_1 and T_2 , ΔH° is the enthalpy change, and ΔS° is the entropy change in a given process.

3. Results and Discussion

3.1. Characterization of Purified and Alkali-Activated Diatomite Samples. As can be seen from Table 2, both the purified and alkali-activated diatomite samples mainly consist of O, Si, Al, and Fe. Alkali-activated diatomite has a lower O and Si content than purified diatomite, and this is probably due to the removal of organic constituents and the dissolution of SiO_2 during alkali treatment. This decrease entrains the increase in the content of Fe and Al.

Both the purified and alkali-activated diatomite samples have an amorphous structure (Figure 2(a)). The broad peaks at 20–25° are typical for amorphous SiO_2 [1, 32, 37, 39, 51]. The absence of the peak around 27° indicates that the diatomite in our study does not contain quartz crystals like other types of diatomite [1, 26, 30, 32, 35, 37, 39, 40].

The FT-IR spectra of the diatomite samples are similar (Figure 2(b)). The broad absorption bands at 3450 cm^{-1} and 1641 cm^{-1} correspond to the adsorbed H_2O , including interlayer water and hydrogen-bonded water with surface hydroxyl groups. A broad band centered at 1101–1031 cm^{-1} and two bands at 789 cm^{-1} and 465 cm^{-1} correspond to the asymmetric stretching vibration, symmetric stretching, and bending vibration of Si-O-Si bonds, respectively [1, 20]. The peaks observed at 3699 cm^{-1} and 3623 cm^{-1} are assigned to surface hydroxyl groups in diatomite. The peak at 3699 cm^{-1} is attributed to the isolated hydroxyl (Si-OH) on the surface of diatomite [1, 43, 55], while the peak at 3623 cm^{-1} belongs to O-H stretching vibration of the aluminol groups ($\equiv\text{AlOH}$) [55]. Alkali-activated diatomite has high-intensity peaks for O-H stretching, indicating that more isolated hydroxyl groups are present on the surface. The peak at 536 cm^{-1} corresponds to the

stretching vibration of Fe-O [1]. The peak at 1380 cm^{-1} is attributed to some organic substances [20]. The intensity of this peak is lower in alkali-activated diatomite than in purified diatomite samples, indicating the removal of organic substances from purified diatomite during NaOH treatment.

The SEM images show that purified diatomite consists of circular cylinders of a diameter of about 5–7 μm , with small pores on the surface (Figures 3(a) and 3(b)). However, these cylinders are partly shattered, causing the pores to become smaller and even blocked. The alkali-activated diatomite retains its multipore structure, and the pores on the surface become larger after treatment (Figures 3(c) and 3(d)). This change may be the result of the formation of soluble silicates SiO_3^{2-} from SiO_2 [4]. Another reason for this change is probably the removal of organic constituents, leading to the increase in the pore size and hence the increase of the surface area of alkali-activated diatomite.

Figure 4 shows the nitrogen adsorption-desorption isotherms and pore size distribution of the diatomite samples. The diatomite exhibits a type II isotherm and an H3-type hysteresis loop, indicating the presence of macroporous structures with nonuniform size and/or shape [56]. Thus, the morphology of the diatomite consists of a variety of shapes (Figure 3). However, the pore size distribution curves of the diatomite samples demonstrate a uniform pore size with an average diameter of 4.3 nm. The textural properties of the samples are presented in Table 3. According to the Brunauer-Emmett-Teller analysis, the purified diatomite exhibits a large specific surface area of 55.4 m^2/g . This value is consistent with that reported by Son et al. [6] (51 m^2/g) for Phu Yen's diatomite and is much higher than that published in previous works [4, 8, 11, 20, 24, 26, 32, 38, 55] (1.0–27 m^2/g). It can be seen from Table 3 that the specific surface area of alkali-activated diatomite (77.8 m^2/g) is significantly larger than that of purified diatomite. This increase in the surface area results from the removal of organic impurities during the alkali treatment.

The zero charge point of purified diatomite is 5.7 (Figure 5). This pH_{PZC} is similar to that published in the

TABLE 6: Isotherm parameters for the adsorption onto alkali-activated diatomite in the binary systems at different temperatures.

| Dye | Temperature (°C) | n | Freundlich K_F | R^2 | q_{max} (mol·g ⁻¹) | Langmuir K_L | R^2 |
|-----|------------------|-------|-----------------------|--------|----------------------------------|--------------------|--------|
| RB | 30 | 14.68 | 0.25×10^{-3} | 0.5081 | 1.40×10^{-4} | 2.27×10^5 | 0.9983 |
| | 45 | 3.53 | 1.88×10^{-3} | 0.8578 | 1.80×10^{-4} | 0.37×10^5 | 0.9905 |
| MB | 30 | 13.00 | 0.93×10^{-3} | 0.6898 | 4.55×10^{-4} | 5.78×10^5 | 0.9949 |
| | 45 | 7.29 | 2.06×10^{-3} | 0.9288 | 5.59×10^{-4} | 4.36×10^5 | 0.9950 |

TABLE 7: Maximum adsorption capacity of RB and MB of different adsorbents.

| Adsorbent | Adsorption capacity (mg·g ⁻¹) | | References |
|--|---|-------------------------------|------------------|
| | RB | MB | |
| Alkali-activated diatomite | 143.9-142.1* 67.0-86.1** | 228.4-220.7* 145.6-178.9** | The present work |
| Purified diatomite | 105.1-92.2* | — | The present work |
| Diatomite was treated with H ₂ SO ₄ (1 molar) | — | 127 | [37] |
| Purified diatomite | — | 72 | [37] |
| Diatomite was treated with sulfuric acid | — | 126.6 (30°C) | [3] |
| Diatomite was treated with sodium hydroxide | — | 27.86 (25°C) | [4] |
| Sodium alginate/silicone dioxide | — | 148.23 | [49] |
| Tagaran natural clay | — | 131.8 (20°C) | [16] |
| Zeolite 4A | — | 44.35 | [19] |
| AlMCM-41 | 41.9 (25°C)* | 66.5 (25°C)* | [5] |
| α -Ag ₂ WO ₄ /SBA-15 | 150 | — | [50] |
| Co and N comodified mesoporous carbon composites | 141 (25°C) | — | [57] |
| Modified banyan aerial roots | 115.23 | — | [12] |
| Biosorbent prepared from inactivated <i>Aspergillus oryzae</i> cells | 98.59 (293 K) | — | [52] |
| L-Asp capped Fe ₃ O ₄ NPs | 10.44 | — | [19] |
| Silica extracted from rice husk | 6.0-6.87 | — | [18] |

*In single systems and **in binary systems at 30 and 45°C.

literature [6, 11, 21, 22]. However, the pH_{PZC} of alkali-activated diatomite (8.9) is much greater than that of purified diatomite. This increase is probably due to the formation of isolated hydroxyl groups on the surface of the material during alkali treatment.

3.2. Isothermal Studies

3.2.1. Adsorption in Single Systems

(1) *Adsorption of RB onto Purified and Alkali-Activated Diatomite Samples.* Figures 6 and 7 present the Freundlich and Langmuir isothermal models for the adsorption of RB dye onto the diatomite samples at 30 and 45°C. The isothermal parameters obtained from the experimental data and the respective correlation coefficients are listed in Table 4. It can be seen that the experimental points fit the models well with high correlation coefficients (0.9104-0.9955). Table 4 also shows that the maximal RB adsorption capacity of the alkali-activated diatomite sample is greater than that of the purified diatomite sample. Thus, the activation of diatomite with sodium hydroxide enhances the adsorption of the RB

TABLE 8: Thermodynamic parameters for adsorption of RB onto purified diatomite in single systems.

| Temperature (°C) | ΔG° (kJ·mol ⁻¹) | ΔH° (kJ·mol ⁻¹) | ΔS° (J·mol ⁻¹ ·K ⁻¹) |
|------------------|--|--|--|
| 30 | -31.26 | 18.90 | 165.53 |
| 45 | -33.74 | | |

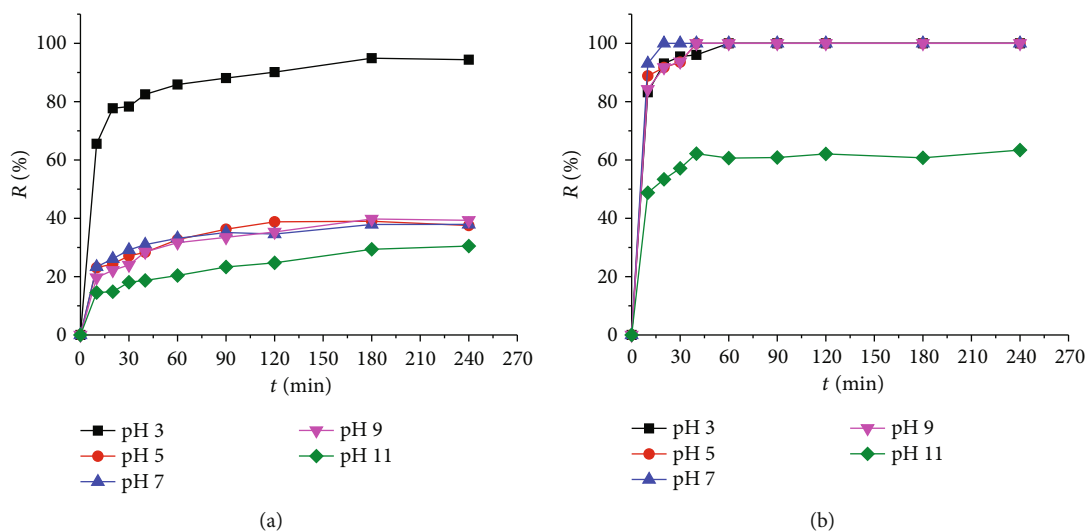
basic dye on diatomite. This enhancement can be attributed to a larger number of the silanol groups formed on the surface, as well as the larger specific surface area of the material.

The results presented above show that alkali-activated diatomite is superior to purified diatomite in terms of chemical and physical properties and adsorption capacity. Therefore, in the following sections, only an alkali-activated diatomite sample is used for the adsorption of dyes from aqueous solutions.

(2) *Adsorption of MB onto Alkali-Activated Diatomite.* The MB adsorption isotherms onto alkali-activated diatomite

TABLE 9: Thermodynamic parameters for the adsorption of the dyes onto alkali-activated diatomite.

| Dye | Temperature (°C) | Single system | | | Binary system | | |
|-----|------------------|--|--|--|--|--|--|
| | | ΔG° (kJ·mol ⁻¹) | ΔH° (kJ·mol ⁻¹) | ΔS° (J·mol ⁻¹ ·K ⁻¹) | ΔG° (kJ·mol ⁻¹) | ΔH° (kJ·mol ⁻¹) | ΔS° (J·mol ⁻¹ ·K ⁻¹) |
| RB | 30 | -30.08 | -11.96 | 59.79 | -31.07 | -96.42 | -215.69 |
| | 45 | -30.98 | | | -27.83 | | |
| MB | 30 | -30.32 | 2.48 | 108.27 | -33.42 | -15.04 | 60.66 |
| | 45 | -31.94 | | | -34.33 | | |

FIGURE 11: Removal efficiency of the dye onto alkali-activated diatomite at different initial solution pHs in the single systems: (a) RB and (b) MB (adsorbent dosage 0.2 g·L⁻¹, initial RB concentration 2.09 × 10⁻⁵ mol · L⁻¹, initial MB concentration 3.13 × 10⁻⁵ mol · L⁻¹, and 30°C).

were also investigated and analyzed according to the linear Freundlich and Langmuir equations. Analysis results are shown in Figure 8 and Table 5. In this case, the Langmuir model is significantly more suitable to describe the adsorption data than the Freundlich model ($R^2 = 0.9874$ - 0.9915 as opposed to $R^2 = 0.7353$ - 0.8676). That is, the adsorption mainly occurs in a monolayer. The maximum adsorption capacity of MB on alkali-activated diatomite is 7.14×10^{-4} and 6.90×10^{-4} (mol·g⁻¹) at 30 and 45°C, respectively.

3.2.2. Adsorption onto Alkali-Activated Diatomite in Binary Systems. Like in the single system, in the binary system, the adsorption of the dyes at 30 or 45°C also follows the Langmuir isothermal model with the R^2 values approaching 1 (Figures 9 and 10). The isothermal data in Table 6 also show that the maximum adsorption capacity of alkali-activated diatomite for MB is higher than that for RB, which is similar to the single systems (Tables 4 and 5). Specifically, the ratio of the maximum adsorption capacity of the dyes in the binary system (MB/RB = $4.55 \times 10^{-4}/1.40 \times 10^{-4} \approx 3.3$ times at 30°C, and MB/RB = $4.55 \times 10^{-4}/1.40 \times 10^{-4} \approx 3.1$ times at 45°C) is higher than that in the single system (MB/RB = $7.14 \times 10^{-4}/3.00 \times 10^{-4} \approx 2.4$ times at 30°C, and MB/RB = $6.90 \times 10^{-4}/2.97 \times 10^{-4} \approx 2.3$ times at 45°C). This proves that there is competitive adsorption in the binary system, where MB molecules preferentially adsorb onto alkali-activated diatomite compared with RB molecules. This enhanced

adsorption might result from the smaller size of the MB molecule. MB molecules more easily diffuse into the pores of diatomite than RB molecules, thus occupying the adsorption sites on the adsorbent surface before the RB molecules do. Similar results are also reported by Eftekhari et al. [5].

Table 7 compares the adsorption capacity of the diatomite samples for RB and MB in this study and that of other adsorbents published in the literature. It can be seen that alkali-activated diatomite has a much higher adsorption capacity than all other adsorbents. Therefore, alkali-activated diatomite might serve as a promising adsorbent for the removal of dyes from aqueous solutions.

3.3. Thermodynamic Studies. The spontaneity of the adsorption process and the interactions on the liquid/solid interface can be explained by using thermodynamic parameters (ΔG° , ΔH° , and ΔS°). If $\Delta G^\circ < 0$, the adsorption process is spontaneous; otherwise, adsorption does not occur on its own. If $\Delta H^\circ < 0$, the adsorption process is exothermic and vice versa. If $\Delta S^\circ > 0$, it is possible to infer that the adsorbent affinity for the dye increases, leading to the increase in randomness of the adsorbates at the liquid/solid interface [4, 42]; in contrast, if $\Delta S^\circ < 0$, more adsorbate molecules adhere to the adsorbent surface [13, 16, 37].

The thermodynamic parameters of RB and MB adsorption onto the diatomite samples are calculated from Equations (9)–(11). The ΔG° of adsorption is negative for both the single and binary systems (Tables 8 and 9), indicating

the spontaneity of adsorption processes. The values of ΔH° and ΔS° differ between the adsorption processes, indicating that the adsorption process is complex. Both the physical and chemical adsorption mechanisms are possible.

3.4. Effect of Solution pH. Figure 11 shows the effect of solution pH on the adsorption of RB and MB onto alkali-activated diatomite in the single system. The pH of the solution was adjusted between 3 and 11 with a 0.1 M HCl or 0.1 M NaOH solution.

As can be seen from Figure 11(a), the adsorption efficiency of RB reaches 94% after 240 min of contact at pH 3. At higher pH, this efficiency decreases drastically, reaching 37% up to pH 5–9 and even lower (30%) at pH 11. We know that RB has a carboxylic group in its molecule, and this group dissociates at higher pHs of the solution. This dissociation renders the molecule negative, resulting in the electric repulsion between RB and the negative surface of the adsorbent at high pH. This result is consistent with that of Eftekhari et al. [5].

For MB (Figure 11(b)), the adsorption efficiency reaches 100% after a short time (60 min) of contact at pH 3–9. The efficiency only decreases to around 60% at pH 11.

The zero charge point of alkali-activated diatomite is 8.9 (Figure 5). Theoretically, the surface of the material is positively charged when $\text{pH} < 8.9$ and negatively charged when $\text{pH} > 8.9$. This means that when the pH of the dye solution increases, the adsorption efficiency should increase because the negatively charged diatomite surface attracts the dye cations. However, in both of our cases, the adsorption efficiency decreases with pH, especially at pH 11. This demonstrates that the adsorption process is complex, and the electrostatic interaction mechanism is not suitable to describe the adsorption of RB and MB onto alkali-activated diatomite.

4. Conclusions

Alkali-activated diatomite is applied to adsorb RB and MB in the single and binary systems. The treatment with sodium hydroxide increases the surface area of the diatomite from $55.4 \text{ m}^2/\text{g}$ to $77.8 \text{ m}^2/\text{g}$ and creates a large number of free silanol groups on the surface of the material. This increases the material's ability to adsorb RB and MB. The adsorption equilibrium data of RB and MB onto alkali-activated diatomite fit the Langmuir model in both the single and binary systems. MB has a higher affinity to the adsorbent than RB, and the binary system is more effective than the single system. The adsorption process is spontaneous, and the removal efficiency of both MB and RB depends on pH significantly.

Data Availability

The data used to support the findings of this study are available from the corresponding author upon request.

Conflicts of Interest

The authors declare that they have no conflicts of interest.

Acknowledgments

This research is funded by Thu Dau Mot University under grant number DT.21.1-018.

References

- [1] D. Dai, H. Liang, D. He, H. Potgieter, and M. Li, "Mn-doped Fe_2O_3 /diatomite granular composite as an efficient Fenton catalyst for rapid degradation of an organic dye in solution," *Journal of Sol-Gel Science and Technology*, vol. 97, no. 2, pp. 329–339, 2021.
- [2] S. J. Allen, G. McKay, and J. F. Porter, "Adsorption isotherm models for basic dye adsorption by peat in single and binary component systems," *Journal of Colloid and Interface Science*, vol. 280, no. 2, pp. 322–333, 2004.
- [3] Z. al-Qodah, W. K. Lafi, Z. al-Anber, M. al-Shannag, and A. Harahsheh, "Adsorption of methylene blue by acid and heat treated diatomaceous silica," *Desalination*, vol. 217, no. 1–3, pp. 212–224, 2007.
- [4] J. Zhang, Q. Ping, M. Niu, H. Shi, and N. Li, "Kinetics and equilibrium studies from the methylene blue adsorption on diatomite treated with sodium hydroxide," *Applied Clay Science*, vol. 83–84, pp. 12–16, 2013.
- [5] S. Eftekhari, A. Habibi-Yangjeh, and S. Sohrabnezhad, "Application of ALMCM-41 for competitive adsorption of methylene blue and rhodamine B: thermodynamic and kinetic studies," *Journal of Hazardous Materials*, vol. 178, no. 1–3, pp. 349–355, 2010.
- [6] B. H. Dang Son, V. Quang Mai, D. Xuan du, N. Hai Phong, and D. Quang Khieu, "A study on Astrazon Black AFDL dye adsorption onto Vietnamese diatomite," *Journal of Chemistry*, vol. 2016, Article ID 8685437, 11 pages, 2016.
- [7] B. H. D. Son, V. Q. Mai, D. X. du, N. H. Phong, N. D. Cuong, and D. Q. Khieu, "Catalytic wet peroxide oxidation of phenol solution over Fe-Mn binary oxides diatomite composite," *Journal of Porous Materials*, vol. 24, no. 3, pp. 601–611, 2017.
- [8] S. K. Padmanabhan, S. Pal, and A. Licciulli, "Diatomite/silver phosphate composite for efficient degradation of organic dyes under solar radiation," *Bulletin of Materials Science*, vol. 43, no. 1, p. 295, 2020.
- [9] Y. L. Zhang, J. Yang, and X. J. Yu, "Preparation, characterization, and adsorption-photocatalytic activity of nano TiO_2 embedded in diatomite synthesis materials," *Rare Metals*, vol. 36, no. 12, pp. 987–991, 2017.
- [10] M. Aivalioti, I. Vamvasakis, and E. Gidarakos, "BTEX and MTBE adsorption onto raw and thermally modified diatomite," *Journal of Hazardous Materials*, vol. 178, no. 1–3, pp. 136–143, 2010.
- [11] J. Chang, J. Zhang, B. Tan, Q. Wang, N. Liu, and Q. Xue, "New insight into the removal of Cd(II) from aqueous solution by diatomite," *Environmental Science and Pollution Research*, vol. 27, no. 9, pp. 9882–9890, 2020.
- [12] H. Fan, Y. Ma, J. Wan, and Y. Wang, "Removal of gentian violet and rhodamine B using banyan aerial roots after modification and mechanism studies of differential adsorption behaviors," *Environmental Science and Pollution Research*, vol. 27, no. 9, pp. 9152–9166, 2020.
- [13] L. C. Paredes-Quevedo, C. González-Caicedo, J. A. Torres-Luna, and J. G. Carriazo, "Removal of a textile azo-dye (basic red 46) in water by efficient adsorption on a natural clay," *Water Air & Soil Pollution*, vol. 232, no. 1, p. 4, 2021.

- [14] Z. H. Yu, S. R. Zhai, H. Guo et al., "Removal of methylene blue over low-cost mesoporous silica nanoparticles prepared with naturally occurring diatomite," *Journal of Sol-Gel Science and Technology*, vol. 88, no. 3, pp. 541–550, 2018.
- [15] V. Vimonses, S. Lei, B. Jin, C. W. K. Chow, and C. Saint, "Kinetic study and equilibrium isotherm analysis of Congo Red adsorption by clay materials," *Chemical Engineering Journal*, vol. 148, no. 2-3, pp. 354–364, 2009.
- [16] B. K. Aziz, D. M. S. Shwan, and S. Kaufhold, "Comparative study on the adsorption efficiency of two different local clays for the cationic dye; application for adsorption of methylene blue from medical laboratories wastewater," *Silicon*, 2021.
- [17] S. Singh, A. Kumar, and H. Gupta, "Activated banana peel carbon: a potential adsorbent for rhodamine B decontamination from aqueous system," *Applied Water Science*, vol. 10, no. 8, p. 185, 2020.
- [18] C. Tsamo, G. D. Kidwang, and D. C. Dahaina, "Removal of rhodamine B from aqueous solution using silica extracted from rice husk," *SN Applied Science*, vol. 2, no. 2, p. 256, 2020.
- [19] N. Belachew, A. Tadesse, M. H. Kahsay, D. S. Meshesha, and K. Basavaiah, "Synthesis of amino acid functionalized Fe₃O₄ nanoparticles for adsorptive removal of rhodamine B," *Applied Water Science*, vol. 11, no. 2, p. 33, 2021.
- [20] Y. Liu, J. Zhang, X. Sheng, N. Li, and Q. Ping, "Adsorption and release kinetics, equilibrium, and thermodynamic studies of hymexazol onto diatomite," *ACS Omega*, vol. 5, no. 45, pp. 29504–29512, 2020.
- [21] M. A. al-Ghouti, M. A. M. Khraisheh, S. J. Allen, and M. N. Ahmad, "The removal of dyes from textile wastewater: a study of the physical characteristics and adsorption mechanisms of diatomaceous earth," *Journal of Environmental Management*, vol. 69, no. 3, pp. 229–238, 2003.
- [22] M. A. al-Ghouti, M. A. M. Khraisheh, M. N. M. Ahmad, and S. Allen, "Adsorption behaviour of methylene blue onto Jordanian diatomite: a kinetic study," *Journal of Hazardous Materials*, vol. 165, no. 1-3, pp. 589–598, 2009.
- [23] M. Piri, E. Sepehr, A. Samadi, K. H. Farhadi, and M. Alizadeh, "Contaminated soil amendment by diatomite: chemical fractions of zinc, lead, copper and cadmium," *International Journal of Environmental Science and Technology*, vol. 18, no. 5, pp. 1191–1200, 2020.
- [24] M. B. Nguyen, T. V. Nguyen, G. H. le et al., "High CO Adsorption Performance of CuCl-Modified Diatomites by Using the Novel Method "Atomic Implantation"," *Journal of Chemistry*, vol. 2021, Article ID 9762578, 12 pages, 2021.
- [25] L. Sun, J. Wang, J. Wu et al., "Constructing nanostructured silicates on diatomite for Pb(II) and Cd(II) removal," *Journal of Materials Science*, vol. 54, no. 9, pp. 6882–6894, 2019.
- [26] Z. Xu, G. Ren, Y. Zhu et al., "Selective adsorption of PHC and regeneration of washing effluents by modified diatomite," *Water Science & Technology*, vol. 81, no. 10, pp. 2066–2077, 2020.
- [27] M. A. al-Ghouti, Y. S. al-Degs, M. A. M. Khraisheh, M. N. Ahmad, and S. J. Allen, "Mechanisms and chemistry of dye adsorption on manganese oxides-modified diatomite," *Journal of Environmental Management*, vol. 90, no. 11, pp. 3520–3527, 2009.
- [28] B. Bahramian, F. D. Ardejani, V. Mirkhani, and K. Badii, "Diatomite-supported manganese Schiff base: an efficient catalyst for oxidation of hydrocarbons," *Applied Catalysis A: General*, vol. 345, no. 1, pp. 97–103, 2008.
- [29] D. Quang Khieu, B. H. Dang Son, V. Thi Thanh Chau, P. Dinh du, N. Hai Phong, and N. Thi Diem Chau, "3-Mercaptopropyltrimethoxysilane modified diatomite: preparation and application for voltammetric determination of lead (II) and cadmium (II)," *Journal of Chemistry*, vol. 2017, Article ID 9560293, 10 pages, 2017.
- [30] S. Li, D. Li, F. Su, Y. Ren, and G. Qin, "Uniform surface modification of diatomaceous earth with amorphous manganese oxide and its adsorption characteristics for lead ions," *Applied Surface Science*, vol. 317, pp. 724–729, 2014.
- [31] Q. Y. Dong, Y. C. Fang, B. Tan, A. Ontiveros-Valencia, A. Li, and H. P. Zhao, "Antimonate removal by diatomite modified with Fe-Mn oxides: application and mechanism study," *Environmental Science and Pollution Research*, vol. 28, no. 11, pp. 13873–13885, 2020.
- [32] Y. Fu, X. Xu, Y. Huang, J. Hu, Q. Chen, and Y. Wu, "Preparation of new diatomite-chitosan composite materials and their adsorption properties and mechanism of Hg(II)," *Royal Society Open Science*, vol. 4, no. 12, p. 170829, 2017.
- [33] N. Ediz, İ. Bentli, and İ. Tatar, "Improvement in filtration characteristics of diatomite by calcination," *International Journal of Mineral Processing*, vol. 94, no. 3-4, pp. 129–134, 2010.
- [34] X. Yang, Y. Zhang, L. Wang, L. Cao, K. Li, and A. Hursthouse, "Preparation of a thermally modified diatomite and a removal mechanism for 1-naphthol from solution," *Water*, vol. 9, no. 9, p. 651, 2017.
- [35] O. Şan, R. Gören, and C. Özgür, "Purification of diatomite powder by acid leaching for use in fabrication of porous ceramics," *International Journal of Mineral Processing*, vol. 93, no. 1, pp. 6–10, 2009.
- [36] G. Zhang, D. Cai, M. Wang, C. Zhang, J. Zhang, and Z. Wu, "Microstructural modification of diatomite by acid treatment, high-speed shear, and ultrasound," *Microporous and Mesoporous Materials*, vol. 165, pp. 106–112, 2013.
- [37] P. Ebrahimi and A. Kumar, "Diatomite chemical activation for effective adsorption of methylene blue dye from model textile wastewater," *International Journal of Environmental Science and Development*, vol. 12, no. 1, pp. 23–28, 2021.
- [38] Y. H. Zhao, J. T. Geng, J. C. Cai, Y. F. Cai, and C. Y. Cao, "Adsorption performance of basic fuchsin on alkali-activated diatomite," *Adsorption Science & Technology*, vol. 38, no. 5-6, pp. 151–167, 2020.
- [39] J. Jin, J. Ouyang, and H. Yang, "One-step synthesis of highly ordered Pt/MCM-41 from natural diatomite and the superior capacity in hydrogen storage," *Applied Clay Science*, vol. 99, pp. 246–253, 2014.
- [40] M. Servatan, M. Ghadiri, M. K. Yazdi et al., "Synthesis of cost-effective hierarchical MFI-type mesoporous zeolite: introducing diatomite as silica source," *Silicon*, 2020.
- [41] E. P. Simonenko, N. P. Simonenko, M. A. Zharkov et al., "Preparation of high-porous SiC ceramics from polymeric composites based on diatomite powder," *Journal of Materials Science*, vol. 50, no. 2, pp. 733–744, 2015.
- [42] S. Zhang, M. Cui, Y. Zhang, Z. Yu, and C. Meng, "Synthesis of zeolite Y from diatomite and its modification by dimethylglyoxime for the removal of Ni(II) from aqueous solution," *Journal of Sol-Gel Science and Technology*, vol. 80, no. 1, pp. 215–225, 2016.
- [43] P. Yuan, D. Q. Wu, H. P. He, and Z. Y. Lin, "The hydroxyl species and acid sites on diatomite surface: a combined IR and Raman study," *Applied Surface Science*, vol. 227, no. 1-4, pp. 30–39, 2004.

- [44] R. Shyam, J. K. Puri, H. Kaur, R. Amutha, and A. Kapila, "Single and binary adsorption of heavy metals on fly ash samples from aqueous solution," *Journal of Molecular Liquids*, vol. 178, pp. 31–36, 2013.
- [45] T. Mahmood, M. T. Saddique, A. Naeem, P. Westerhoff, S. Mustafa, and A. Alum, "Comparison of different methods for the point of zero charge determination of NiO," *Industrial & Engineering Chemistry Research*, vol. 50, no. 17, pp. 10017–10023, 2011.
- [46] H. P. Jing, C. C. Wang, Y. W. Zhang, P. Wang, and R. Li, "Photocatalytic degradation of methylene blue in ZIF-8," *RSC Advances*, vol. 4, no. 97, pp. 54454–54462, 2014.
- [47] P. Dinh du and P. Ngoc Hoai, "Synthesis of MIL-53(Fe) metal-organic framework material and its application as a catalyst for Fenton-type oxidation of organic pollutants," *Advances in Materials Science and Engineering*, vol. 2021, Article ID 5540344, 13 pages, 2021.
- [48] O. Hamdaoui and E. Naffrechoux, "Modeling of adsorption isotherms of phenol and chlorophenols onto granular activated carbon: Part I. Two-parameter models and equations allowing determination of thermodynamic parameters," *Journal of Hazardous Materials*, vol. 147, no. 1-2, pp. 381–394, 2007.
- [49] H. Hosseinzadeh and K. Abdi, "Efficient removal of methylene blue using a hybrid organic-inorganic hydrogel nanocomposite adsorbent based on sodium alginate-silicone dioxide," *Journal of Inorganic and Organometallic Polymers and Materials*, vol. 27, no. 6, pp. 1595–1612, 2017.
- [50] F. C. M. Silva, L. K. R. Silva, A. G. D. Santos et al., "Structural refinement, morphological features, optical properties, and adsorption capacity of α -Ag₂WO₄ nanocrystals/SBA-15 mesoporous on rhodamine B dye," *Journal of Inorganic and Organometallic Polymers and Materials*, vol. 30, no. 9, pp. 3626–3645, 2020.
- [51] P. Liu, T. Chen, and J. G. Zheng, "Removal of iodate from aqueous solution using diatomite/nano titanium dioxide composite as adsorbent," *Journal of Radioanalytical and Nuclear Chemistry*, vol. 324, no. 3, pp. 1179–1188, 2020.
- [52] F. H. M. Souza, V. F. C. Leme, G. O. B. Costa, K. C. Castro, T. R. Giralddi, and G. S. S. Andrade, "Biosorption of rhodamine B using a low-cost biosorbent prepared from inactivated *Aspergillus oryzae* cells: kinetic, equilibrium and thermodynamic studies," *Water Air & Soil Pollution*, vol. 231, no. 5, p. 242, 2020.
- [53] N. L. My Linh, D. Hoang van, T. Duong, M. X. Tinh, and D. Quang Khieu, "Adsorption of arsenate from aqueous solution onto modified Vietnamese bentonite," *Advances in Materials Science and Engineering*, vol. 2019, Article ID 2710926, 13 pages, 2019.
- [54] N. Thi Huong, N. N. Son, V. H. Phuong, C. T. Dung, P. T. M. Huong, and L. T. Son, "Synthesis Fe₃O₄/talc nanocomposite by coprecipitation-ultrasonication method and advances in hexavalent chromium removal from aqueous solution," *Adsorption Science & Technology*, vol. 38, no. 9-10, pp. 483–501, 2020.
- [55] S. C. Ma, Z. G. Wang, J. L. Zhang, D. H. Sun, and G. X. Liu, "Detection analysis of surface hydroxyl active sites and simulation calculation of the surface dissociation constants of aqueous diatomite suspensions," *Applied Surface Science*, vol. 327, pp. 453–461, 2015.
- [56] G. Leofanti, M. Padovan, G. Tozzola, and B. Venturelli, "Surface area and pore texture of catalysts," *Catalysis Today*, vol. 41, no. 1-3, pp. 207–219, 1998.
- [57] Z. Zheng, Q. Liu, and F. Wang, "In-situ carbonization of ZIF-67 to fabricate magnetically Co/N-mC with high adsorption capacity toward water remediation," *SN Applied Sciences*, vol. 3, no. 1, p. 111, 2021.